Inorganic Chemistry

Article

pubs.acs.org/IC

Thermochemistry of $Sr_2Ce_{1-x}Pr_xO_4$ (x = 0, 0.2, 0.5, 0.8, and 1): Variable-Temperature and -Atmosphere in-situ and ex-situ Powder X-ray Diffraction Studies and Their Physical Properties

Wang Hay Kan and Venkataraman Thangadurai*

Department of Chemistry, University of Calgary, 2500 University Drive Northwest, Calgary, Alberta T2N 1N4, Canada

Supporting Information

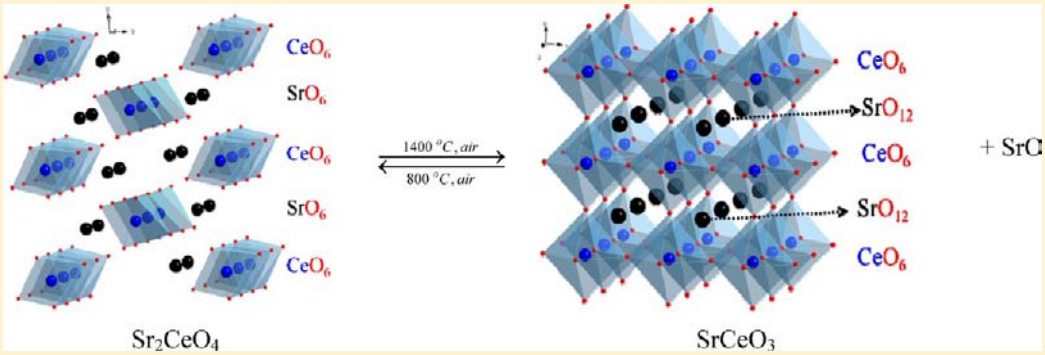

ABSTRACT: A novel family of metal oxides with a chemical formula of $Sr_2Ce_{1-x}Pr_xO_4$ (x = 0, 0.2, 0.5, 0.8, and 1) was developed as mixed oxide ion and electronic conductors for solid oxide fuel cells (SOFCs). All of the investigated samples were synthesized by the ceramic method at 1000 °C in air and characterized by powder X-ray diffraction (PXRD), selected area electron diffraction (SAED), thermogravimetric analysis (TGA), scanning electron microscopy (SEM), energy-dispersive X-ray spectroscopy (EDX), and electrochemical impedance spectroscopy (EIS). Ex-situ PXRD reveals that the Sr_2PbO_4-type Sr_2CeO_4 decomposes readily into a mixture of perovskite-type $SrCeO_3$ and rock-salt-type SrO at 1400 °C in air. Surprisingly, the decomposed products are converted back to the original Sr_2PbO_4-type Sr_2CeO_4 phase at 800 °C in air, as confirmed by in-situ PXRD. Thermal decomposition is highly suppressed in $Sr_2Ce_{1-x}Pr_xO_4$ compounds for Pr > 0, suggesting that Pr improves the thermal stability of the compounds. Rietveld analysis of PXRD and SAED supported that both Pr and Ce ions are located on the *2a* site in *Pbam* (space group no. 55). The electrical transport mechanism could be correlated to the reduction of Pr and/or Ce ions and subsequent loss of oxide ions at elevated temperatures, as shown by TGA and in-situ PXRD. Conductivity increases with Pr content in $Sr_2Ce_{1-x}Pr_xO_4$. The highest total conductivity of 1.24×10^{-1} S cm^{-1} was observed for $Sr_2Ce_{0.2}Pr_{0.8}O_4$ at 663 °C in air.

1. INTRODUCTION

Strontium cerium oxide Sr_2CeO_4 with Sr_2PbO_4-type structure is one of the most promising blue emission phosphors, which was first developed by Danielson et al. in 1998.[1,2] The emission mechanism involves UV-induced excitation of electrons from the terminal O^{2-} ions to Ce^{4+} ions and subsequent electron transition from Ce^{3+} ions to O^{2-} ions with a long excited-state lifetime of ca. 50 μs.[3] To our best of knowledge, such luminescence property is not observed in other Ce^{4+}-based systems, e.g., perovskite-type $ACeO_3$ (A = alkaline earth), suggesting that the mixed Ce^{3+}/Ce^{4+} ions are stabilized in the Sr_2PbO_4-type structure.[4] Masui et al. observed Ce^{3+} species on the surface of Sr_2CeO_4 particles by XPS.[4] Albeit, Sr_2CeO_4 phase seems to possess cell parameters relationship of the layered Ruddlesdon-Popper phase Sr_2TiO_4,[5,6] it belongs to the Sr_2PbO_4-type structure.[2,7] The Sr_2PbO_4-type structure consists of unusual 1-dimensional chains of edge-shared CeO_6 octahedra along [001],[8,9] unlike the 2-dimensional edge-shared octahedra TiO_6 planes in Sr_2TiO_4 (*I*4/*mmm*, space group no. 139).[5,6] Moreover, the CeO_6 octahedra in Sr_2CeO_4 are slightly distorted and contain asymmetric Ce−O axial and equatorial distances of ca. 2.23 and ca. 2.35 Å, respectively, in contrast to the Ce−O of ca. 2 Å in the highly symmetric CeO_6 octahedra in the simple/double-perovskite (e.g., $BaCeO_3$ and $Ba_3Ca_{1.18}Nb_{1.82}O_{9-\delta}$). The Ce−Ce distance in Sr_2CeO_4 (ca. 3.5 Å) is about 0.5 Å shorter than that in $SrCeO_3$.[2,3]

We anticipate that the short Ce−Ce distance may promote fast electrical conduction when Ce^{4+} are partially reduced to Ce^{3+} at elevated temperatures.[10−12] The mixed Ce^{3+}/Ce^{4+} ions could also facilitate hydrocarbons (e.g., CH_4 and H_2) oxidation[10,11,13] and, therefore, are highly desirable as mixed conductors for solid oxide fuel cells (SOFCs).[14−16] In addition, the electrical transport properties can be further improved through substitution of Ce^{4+} ion with Pr^{4+} ions, which have a lower reduction potential than that of Ce ions.[17] Formation of

Received: May 23, 2012
Published: August 1, 2012

   dx.doi.org/10.1021/ic301071x | Inorg. Chem. 2012, 51, 8973−8981

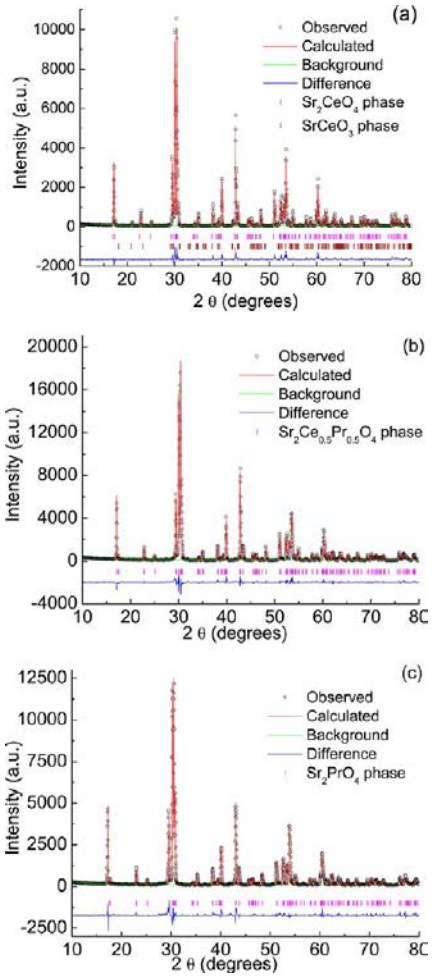

Figure 1. PXRD Rietveld refinement plots of the as-prepared (a) Sr_2CeO_4, (b) $Sr_2Ce_{0.5}Pr_{0.5}O_4$, and (c) Sr_2PrO_4.

the thermodynamically stable perovskite-type $SrCeO_3$ is favorable over Sr_2CeO_4 in the $SrO-CeO_2$ system. As-prepared Sr_2CeO_4 is stable under ambient atmosphere for a few weeks, but it is slowly converted into $SrCeO_3$ phase.[18] Furthermore, Sr_2CeO_4 is chemically unstable in pure CO_2 at elevated temperatures and formed $SrCO_3$ and CeO_2 phases.[7] The synthetic method of Sr_2CeO_4 phase is extensively studied, including conventional mixed oxide solid-state reactions,[1,2] chemical coprecipitation,[4,19,20] Pechini's polymerization,[21−23] laser ablation,[24−26] sol−gel methods,[27−29] combustion methods,[30−32] emulsion liquid membrane systems,[33−35] and hydrothermal synthesis and microwave methods.[19,36,37] These studies focus on understanding the role of doping strategy and the corresponding luminescent property. Interestingly, the isostructural Sr_2PrO_4 compound does not exhibit luminescence property over the wavelength range of 250−750 nm.[38−40]

In this work, a new family of $Sr_2Ce_{1-x}Pr_xO_4$ (x = 0, 0.2, 0.5, 0.8, and 1) was developed as potential mixed conductors for solid oxide fuel cells (SOFCs). In-situ and ex-situ powder X-ray diffraction (PXRD), selected area electron diffraction (SAED), thermogravimetric analysis (TGA), scanning electron microscopy (SEM), energy-dispersive X-ray spectroscopy (EDX), and electrochemical impedance spectroscopy (EIS) were used to understand the thermophysical properties of $Sr_2Ce_{1-x}Pr_xO_4$. Ex-situ PXRD and other physical methods reveal further insight into the chemical stability and physical properties of the Pr-doped Sr_2CeO_4.

2. EXPERIMENTAL SECTION

2.1. Synthesis of $Sr_2Ce_{1-x}Pr_xO_4$. $Sr_2Ce_{1-x}Pr_xO_4$ (x = 0, 0.2, 0.5, 0.8, 1) were synthesized by the conventional solid-state method using stoichiometric amounts of $SrCO_3$ (99+%, Alfa Aesar), CeO_2 (99+%, Alfa Aesar), and Pr_6O_{11} (99+%, Alfa Aesar). The reactant powders were ball milled (Pulverisette, Fritsch, Germany) in 2-propanol using a ZrO_2 ball for 6 h at 200 rpm. Precursors were dried and

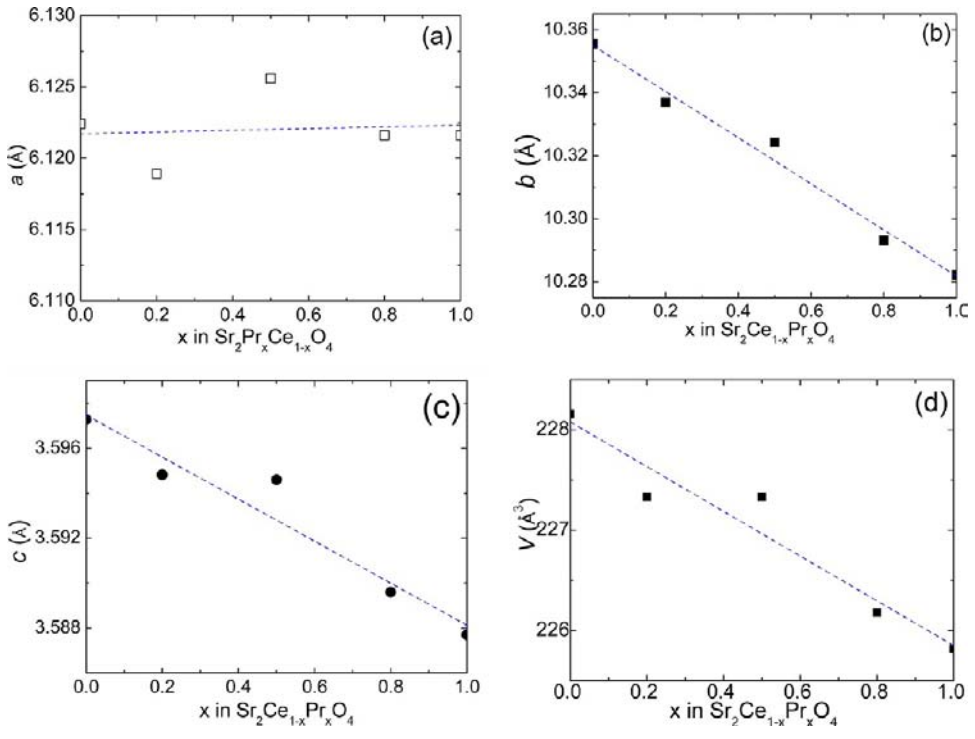

Figure 2. Cell parameters (a−c) and (d) unit cell volumes of the as-prepared $Sr_2Ce_{1-x}Pr_xO_4$.

dx.doi.org/10.1021/ic301071x | Inorg. Chem. 2012, 51, 8973−8981

Table 1. Structural Solution of the Rietveld Refinement of the As-Prepared Sr_2CeO_4, $Sr_2Ce_{0.8}Pr_{0.2}O_4$, $Sr_2Ce_{0.5}Pr_{0.5}O_4$, $Sr_2Ce_{0.2}Pr_{0.8}O_4$, and Sr_2PrO_4

	Sr_2CeO_4[a]	$Sr_2Ce_{0.8}Pr_{0.2}O_4$	$Sr_2Ce_{0.5}Pr_{0.5}O_4$	$Sr_2Ce_{0.2}Pr_{0.8}O_4$	Sr_2PrO_4
Sr (*4h*) occup	1	1	1	1	1
x	0.0635(2)	0.0622(3)	0.0626(2)	0.0616(4)	0.0634(3)
y	0.6797(2)	0.6791(2)	0.6788(1)	0.6779(3)	0.6788(2)
z	0.5	0.5	0.5	0.5	0.5
U_{iso} (100 × Å^2)	0.29(7)	0.38(7)	0.40(6)	0.3(1)	0.33(8)
Ce/Pr (*2a*) occup	1/0	0.2/0.8	0.5/0.5	0.8/0.2	0/1
x	0	0	0	0	0
y	0	0	0	0	0
z	0	0	0	0	0
U_{iso} (100 × Å^2)	0.29(7)	0.4(4)	0.44(6)	0.3(1)	0.42 (8)
O1 (*4g*) occup	1	1	1	1	1
x	0.854(2)	0.856(2)	0.858(1)	0.861(3)	0.871(2)
y	0.804(1)	0.801(1)	0.7985(8)	0.800(2)	0.802(1)
z	0	0	0	0	0
U_{iso} (100 × Å^2)	0.2(3)	0.3(3)	0.2(2)	0.1(6)	0.4(3)
O2 (*4h*) occup	1	1	1	1	1
x	0.233(1)	0.237(1)	0.235(1)	0.240(3)	0.232(2)
y	−0.0438(9)	−0.045(1)	−0.045(1)	−0.045(2)	−0.0435(9)
z	0.5	0.5	0.5	0.5	0.5
U_{iso} (100 × Å^2)	0.2(3)	0.4(4)	0.4(3)	0.4(6)	0.4(3)
R_p (%)	5.75	8.50	7.38	13.61	8.58
a (Å)	6.12240(7)	6.1189(1)	6.1256(2)	6.1216(3)	6.1216(2)
b (Å)	10.3555(1)	10.3369(2)	10.3242(3)	10.2932(6)	10.2822(3)
c (Å)	3.59728(5)	3.59482(8)	3.5946(1)	3.5896(2)	3.5877(1)
V (Å^3)	228.161(7)	227.33(2)	227.33(2)	226.18(4)	225.82(2)

[a]As-prepared Sr_2CeO_4 consists of ∼95% of Sr_2CeO_4 and ∼5% of $SrCeO_3$. Detailed structural solution of the PXRD Rietveld refinement result is summarized in Table S1, Supporting Information.

subsequently calcinated at 1000 °C in air for 12 h at a 5 °C/min ramp rate. Resulting powders were hand grinded and pressed into pellets using an isostatic pressure of ca. 200 M Pa. Pellets were sintered at 1000 °C in air for 12 h at a 5 °C/min ramp rate. The single-crystalline $Sr(OH)_2{\cdot}8H_2O$ compound was prepared by the ambient crystallization method in water. As-prepared Sr_2CeO_4 powder was sintered at 1400 °C in air for 4 h, and the postsintered sample (ca. 1 g) was put into a 20 mL glass vial with 10 mL of water. The single-crystalline compound was obtained from the solution mixture in ca. 2 weeks at room temperature.

2.2. Phase Characterization. Ex-situ powder X-ray diffraction (PXRD) measurement was carried out in a Bruker D8 Advance powder X-ray diffractometer (Cu Kα, 40 kV, 40 mA). Typically, solid phases were measured from 2θ = 10° to 2θ = 80° at a count rate of 15 s per step of 0.02° at ambient condition. For thermal stability measurements, the samples were heated to the target temperatures at a ramp rate of 10 °C/min. Samples were cooled down to room temperature prior to ex-situ PXRD measurement. In-situ PXRD measurements were performed in same Bruker diffractometer with a high-temperature reactor chamber (Anton Paar XRK 900) attached. Samples were measured from 2θ = 10° to 2θ = 80° at a count rate of 3 s per step of 0.05°.

For the thermal stability measurements, the samples were heated to the target temperatures at a ramp rate of 6 °C/min and stabilized in various reactive gases for 30 min prior to measurements. In-situ and ex-situ PXRD data sets were refined by the conventional Rietveld method using the GSAS package with the EXPGUS interface.[41] Background, scale factor, zero-point position, cell parameters, atomic positions, and profile coefficients for Pseudo-Voight/FCJ Asymmetric peak shape function were refined until convergence was achieved. Bond lengths were obtained by the DISAGL Version Win32 Crystal Structure Distance and Angle Program in the GSAS packet on XRD data sets.[41] Bond valences of Sr ions were calculated by Bond Valence Calculator Version 2.00.[42,43] However, the bond valences of Pr^{4+} and Ce^{4+} ions were not calculated due to the lack of certain bond valence parameters r_o.[42,44−47] Nonetheless, the Pr/Ce−O bond lengths were calculated and reported. Single-crystalline compounds were measured in an Oxford Diffraction Gemini A Ultra single X-ray diffractometer equipped with Nonius Kappa CCD. The structure was solved and refined by SHELXTL.[48]

Microstructures of the samples were analyzed in a Philips XL 30 conventional scanning electron microscope (SEM) equipped with an energy-dispersive X-ray spectrometer (EDX). Samples were gold coated beforehand to prevent the surface charging effect. Images were recorded at 20 kV with a secondary electron detector. Selected area electron diffraction (SAED) was performed on a FEI Tecnai F20 FEG-TEM (FEI, Eindhoven, The Nethelands) equipped with a Gatan Imaging Filter and a Gatan 860 GIF 2001 CCD of 1024 × 1024 resolution. Thermal stability measurement was conducted in a METTLER TOLEDO thermal system TGA/DSC1 (HT 1600 °C) Thermogravimetric Analyzer with a Star^e system. Samples were measured up to 800 °C at a ramping rate of 10 °C/min.

2.3. Electrical Characterization. Electrical properties were measured by electrochemical impedance spectroscopy (EIS). The as-prepared samples were pelletized (isostatic pressure of ca. 200 M Pa) and sintered at 1400 °C for 14 h. Both sides of the pellets were Pt coated (Heraeus Inc., LP A88-11S, Germany) and stabilized at 900 °C for 1 h to remove organic binders. Pt wires were attached to the surface of the pellet using spring-loaded contact which served as current collectors. The cell was then heated to the temperature range 200−800 °C using a Barnstead tubular furnace (model no. 21100) and held at constant temperatures for 2 h prior to each measurement. EIS (Solartron Electrochemical Impedance Spectroscopy; SI model no. 1260, 100 mV, 0.01 Hz to 1 MHz) was recorded in two-probe electrochemical cells. Measurements were made for both heating and cooling cycles to ensure reproducibility.

dx.doi.org/10.1021/ic301071x | Inorg. Chem. 2012, 51, 8973−8981

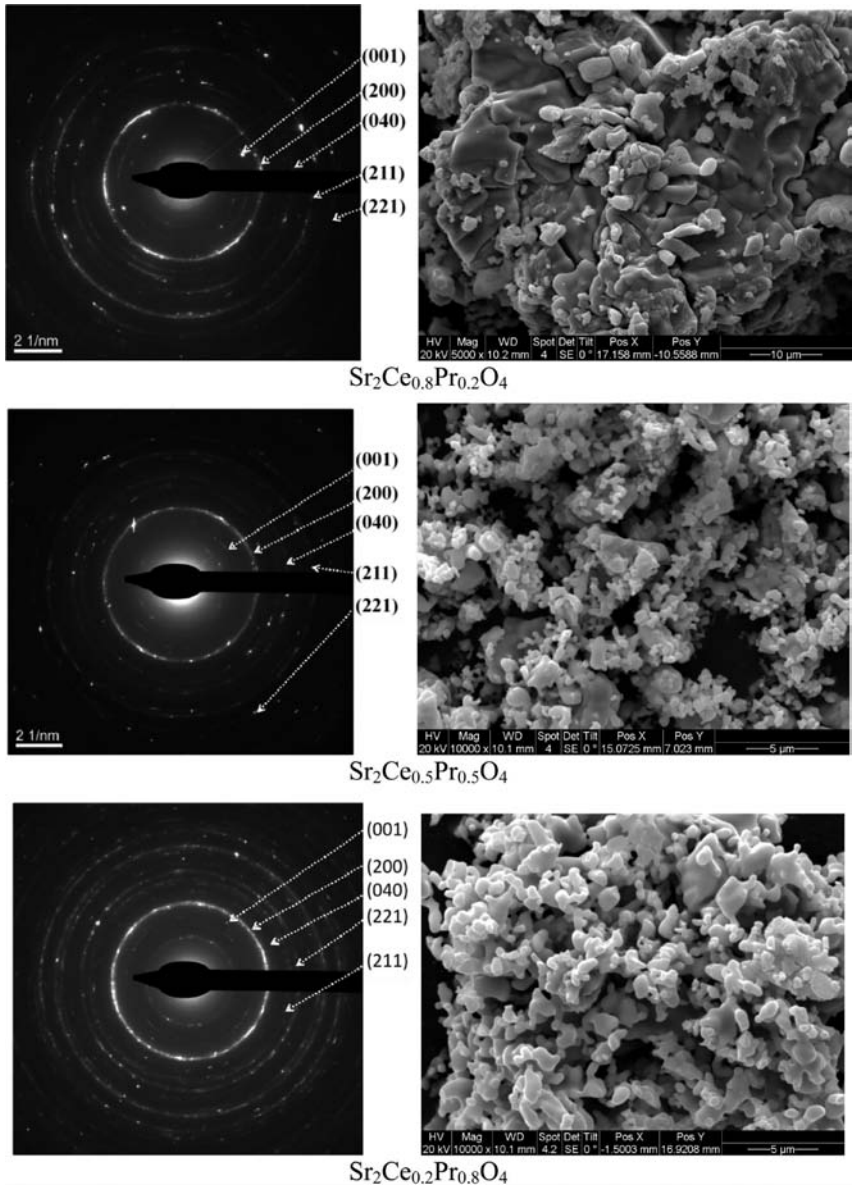

Figure 3. Selected area electron diffraction (SAED) and scanning electron microscopy images (SEM) of the as-prepared $Sr_2Ce_{1-x}Pr_xO_4$ (x = 0.2, 0.5, and 0.8).

3. RESULTS AND DISCUSSION

3.1. Structural Analysis. All of the as-prepared $Sr_2Ce_{1-x}Pr_xO_4$ (x = 0, 0.2, 0.5, 0.8, 1) samples are phase pure and can be indexed as *Pbam* in the PXRD patterns. However, a trace amount (3.17%) of perovskite-type $SrCeO_3$ (Joint Committee on Powder Diffraction Standards (JCPDS) Card No. 01-89-5546) was detected in the Sr_2CeO_4 sample. We modified Danielson's previous structural solution of Sr_2CeO_4 for $Sr_2Ce_{1-x}Pr_xO_4$ by allowing both Pr^{4+} and Ce^{4+} atoms located on the same *2a* site.[1] New structural solutions were verified by applying the Rietveld refinement to the PXRD data as shown in Figure 1. Cell volumes of the compounds follow Vegard's law, in which the volumes decrease with the Pr content as shown in Figure 2.[49] The result indicates that Pr atoms form a complete solid solution with Ce atoms on the *2a* site for the entire range of x (from 0 to 1) in $Sr_2Ce_{1-x}Pr_xO_4$. Similar to Danielson's model,[1] Sr atoms were set to locate on the *4h* site while O atoms were set to locate on *4g* and *4h* sites for $Sr_2Ce_{1-x}Pr_xO_4$. Detailed structural solutions of the Rietveld refinement of the as-prepared samples are summarized in Table 1. Bond valence sum calculations further confirm the valences of Sr^{2+} cations in the compounds in Figure S1, Supporting Information. Calculated bond lengths of Sr−O and Ce/Pr−O are found to be consistent with the literature.[1,38] Selected area electron diffraction (SAED) images support the Rietveld solutions in which all of the Debyes rings can be indexed accordingly, as shown in Figure 3. Samples are found to be very homogeneous in size, in the range of a few micrometers, in the scanning electron microscopy (SEM) images. Energy-dispersive X-ray spectroscopy (EDX) confirms the elemental ratios of the samples as shown in Table S2, Supporting Information.

3.2. Thermochemistry of $Sr_2Ce_{1-x}Pr_xO_4$. The thermal stability of Sr_2CeO_4 is accessed by ex-situ and in-situ PXRD. Ex-situ PXRD measurement indicates that Sr_2CeO_4 phase is thermally stable up to 1350 °C in air, as shown in Figure 4a. Lattice constants were found to be consistent from 1000 to 1350 °C in Figure 4b−d. However, a mixture of newly formed SrO (JCPDS Card No. 01-075-0263) and $SrCeO_3$ (JCPDS

dx.doi.org/10.1021/ic301071x | Inorg. Chem. 2012, 51, 8973−8981

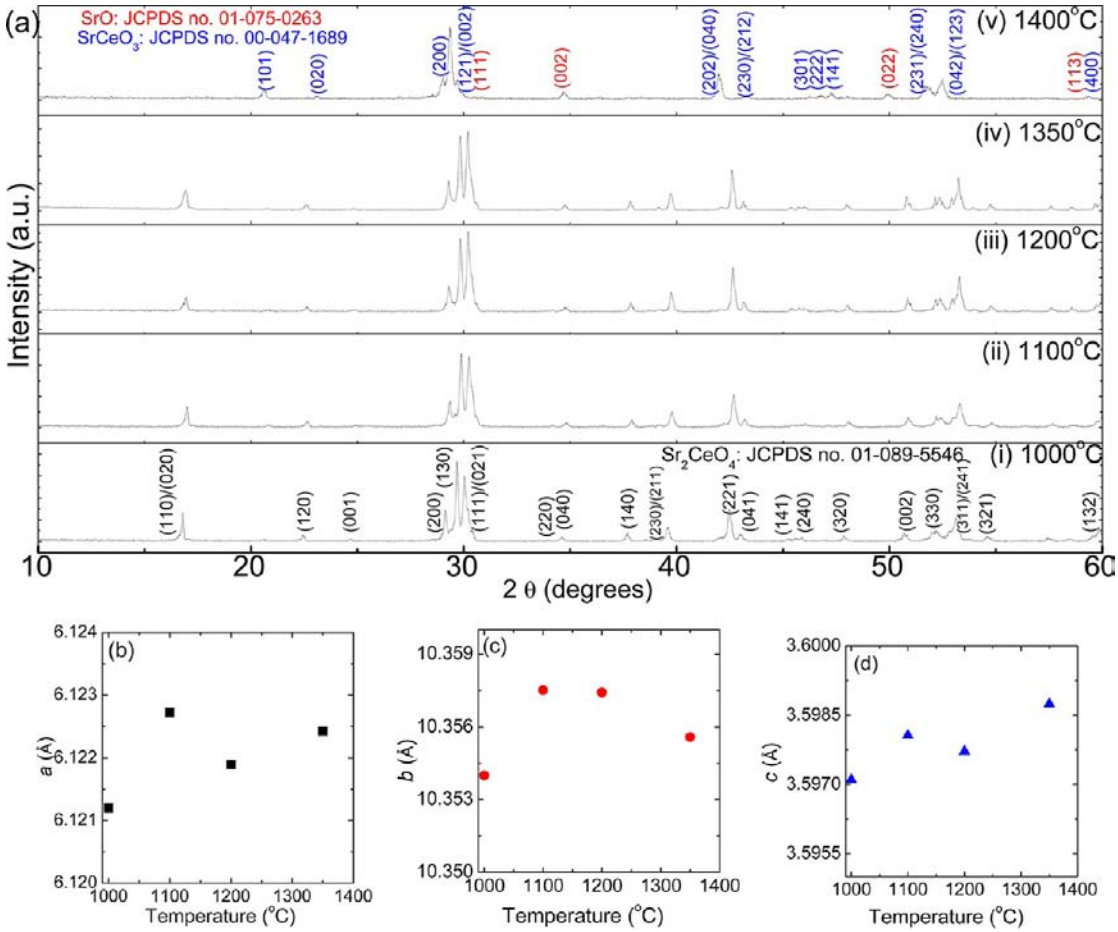

Figure 4. (a) Ex-situ PXRD analysis shows the structural transformation of Sr_2CeO_4 (JCPDS no. 01-089-5546) into perovskite-type $SrCeO_3$ (JCPDS no. 01-075-0263) and SrO (JCPDS no. 00-047-1689) in air. (b–d) Lattice parameters of Sr_2CeO_4 samples after heat treatment at elevated temperatures indicate that the structures are unchanged up to 1350 °C.

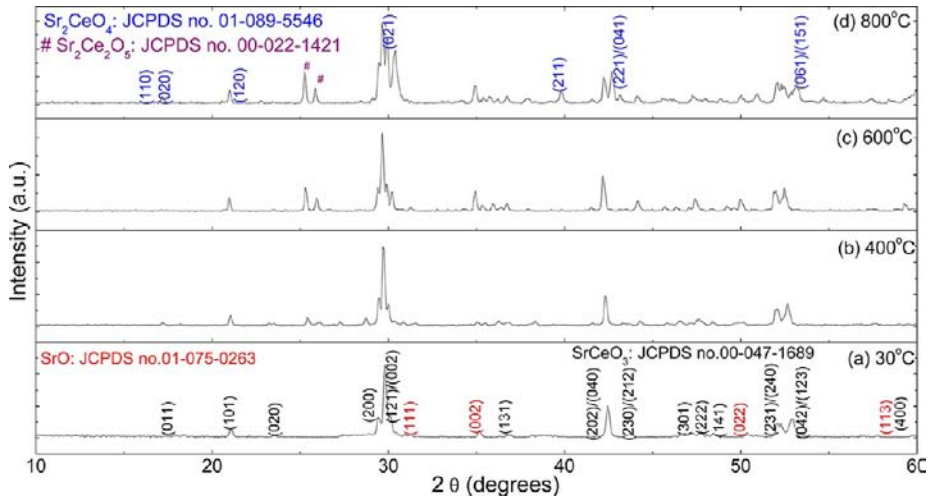

Figure 5. In-situ PXRD analysis showing the reverse structural transformation of perovskite $SrCeO_3$ (JCPDS no. 00-047-1689) and SrO (JCPDS no. 01-075-0263) into Sr_2PbO_4-type Sr_2CeO_4 (JCPDS no. 01-089-5546) at elevated temperatures in air.

Card No. 01-89-5546) were observed at 1400 °C in air, while the characteristic PXRD peaks of Sr_2CeO_4 were absent (Figure 4a(v)).[50,51] Interestingly, the decomposed products can be converted back to the original Sr_2CeO_4 phase in situ at 800 °C in air, indicating that Sr_2CeO_4 phase is a metastable phase as confirmed by in-situ PXRD in Figure 5. Conversely, thermal decomposition is highly suppressed in all Pr-substituted $Sr_2Ce_{1-x}Pr_xO_4$ at 1400 °C in air in Figure 6, suggesting that Pr ions seem to improve the structural stability of the compounds. Cell constants of the as-prepared samples were compared before and after heat treatments at 1400 °C in air; it was found that comparable cell constants were obtained, which

dx.doi.org/10.1021/ic301071x | Inorg. Chem. 2012, 51, 8973–8981

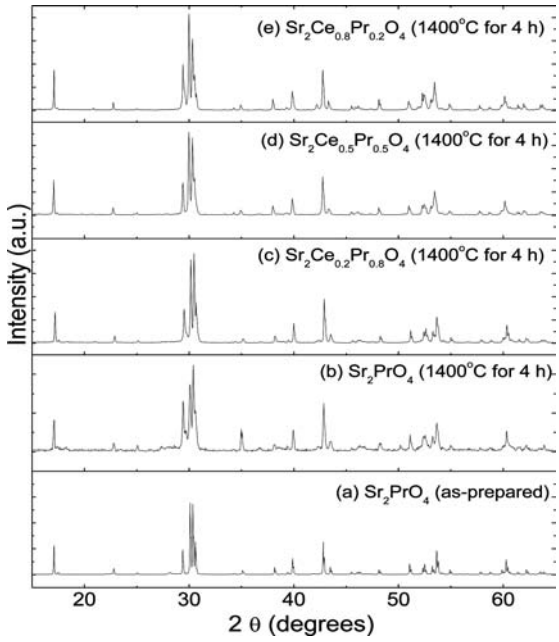

Figure 6. Ex-situ PXRD patterns of $Sr_2Ce_{1-x}Pr_xO_4$ (x = 0.2, 0.5, 0.8, 1) at 1400 °C for 4 h.

further support the thermal stability of Pr-containing compounds (Table S3, Supporting Information).

The thermally decomposed products of SrO and $SrCeO_3$ are further confirmed by the fact that a single crystal of $Sr(OH)_2{\cdot}8H_2O$ can be produced in water in ambient condition. The corresponding single-crystal refinement is summarized in Table S4, Supporting Information. The structure of the crystal was found to be reported previously by Harr in 1947.[52] However, a very different synthetic route was used in the current study in which the crystals were grown in the presence of a high impurity of $SrCeO_3$. The overall thermochemical properties of Sr_2CeO_4 could be described as

$$Sr_2CeO_{4(s)} \underset{800^\circ C,air}{\overset{1400^\circ C,air}{\rightleftharpoons}} SrCeO_{3(s)} + SrO_{(s)}$$

$$\xrightarrow{25^\circ C,water} SrCeO_{3(s)} + Sr(OH)_2.8H_2O_{(s)}$$

At elevated temperature (300−1000 °C) in reducing atmosphere (10% H_2/N_2), the as-prepared Sr_2CeO_4 phase is structurally stable, based on the in-situ PXRD pattern in Figure 7. All three cell constants increase linearly with temperature, indicating thermal expansion of the unit cells. However, the Pr-rich members, namely, $Sr_2Ce_{0.2}Pr_{0.8}O_4$ and Sr_2PrO_4, show certain structural instability in 10% H_2/N_2; the intensities of the diffraction peaks at 2θ = 16.8° and 2θ = 29.2° (corresponding to (110) and (200) planes) decrease with temperature (Figure 8). We believe that the Pr/Ce reductions could decrease the mosaicity of the diffraction planes where the Pr/CeO_6 edge-shared octahedra chains are located (Figure S2, Supporting Information).[38] Fiscus also showed that Sr_2PrO_4 was completely converted into SrO and Pr_2O_3 phases in 5% H_2/N_2 by TGA and PXRD analyses.[38] In order to improve the chemical stability of the compounds, we are currently

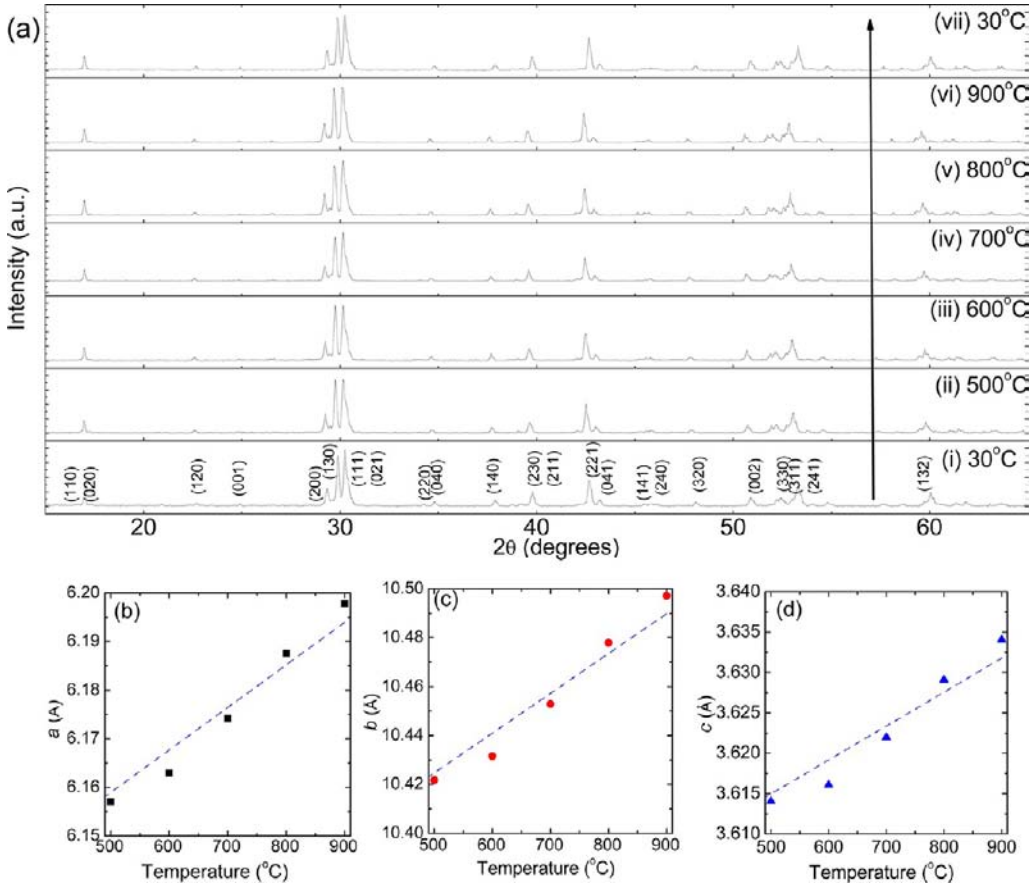

Figure 7. (a) In-situ PXRD patterns and (b−d) corresponding lattice parameters of Sr_2CeO_4 in 10% H_2/N_2 as a function of temperature.

dx.doi.org/10.1021/ic301071x | Inorg. Chem. 2012, 51, 8973−8981

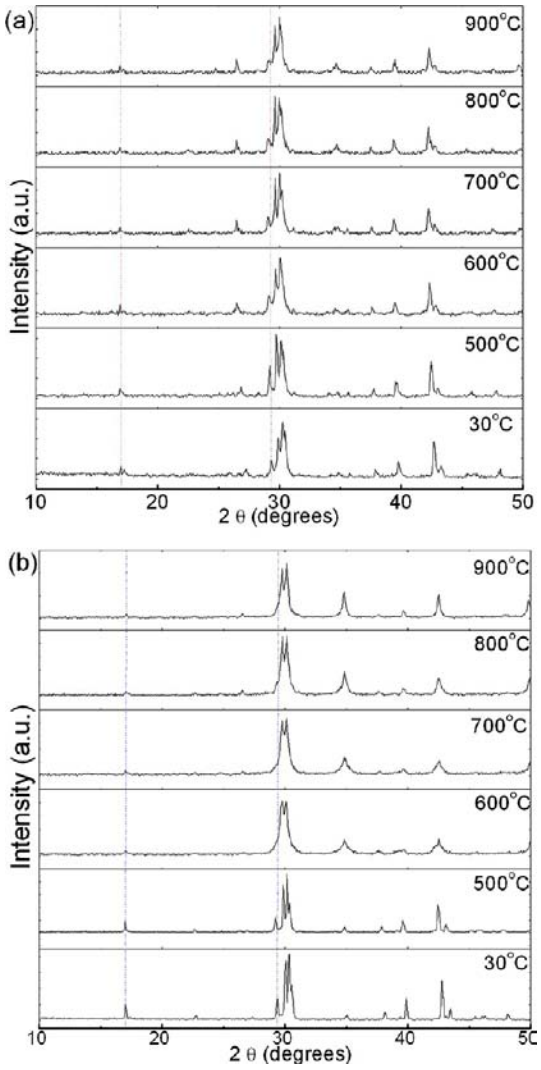

Figure 8. In-situ powder XRD patterns of (a) $Sr_2Ce_{0.2}Pr_{0.8}O_4$ and (b) Sr_2PrO_4 at elevated temperature in 10% H_2/N_2. Measurements were performed in ascending order of temperature.

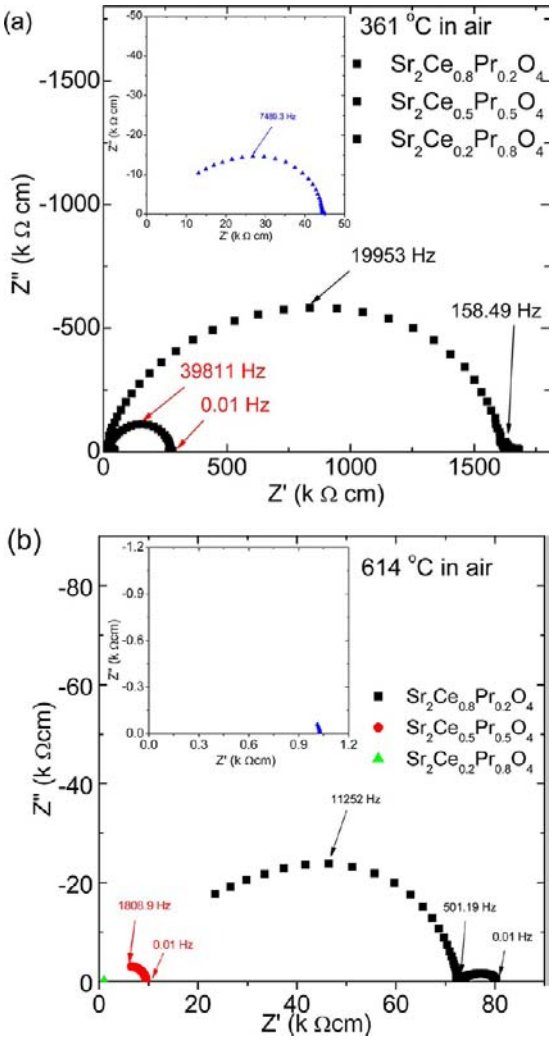

Figure 9. Typical electrochemical impedance spectra of $Sr_2Ce_{1-x}Pr_xO_4$ (x = 0.2, 0.5, 0.8) in air.

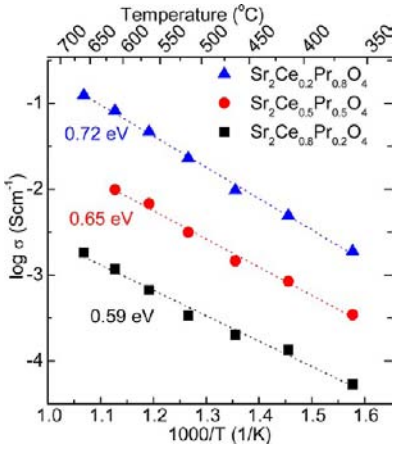

Figure 10. Arrhenius plot of $Sr_2Ce_{1-x}Pr_xO_4$ (x = 0.2, 0.5, 0.8) in air.

conducting further research on the doping effect of Zr and Ti on $Sr_2Ce_{1-x}Pr_xO_4$.[53−55]

3.3. Electrical Properties. The conduction behavior of Sr_2CeO_4 was not reported previously, partially due to the physical instability of the phase at the sintering temperature (≥1400 °C). Conversely, the Pr-containing $Sr_2Ce_{1-x}Pr_xO_4$ was found to be structurally stable up to 1400 °C in air. This provides an essential condition for us to measure the electrical transport behavior of the compounds. We were able to measure $Sr_2Ce_{1-x}Pr_xO_4$ (x = 0.2, 0.5, 0.8). The Sr_2PrO_4 compound could not be sintered at the same temperature (1400 °C). Typical AC EIS plots of $Sr_2Ce_{1-x}Pr_xO_4$ (x = 0.2, 0.5, 0.8) at both low (361 °C) and high (614 °C) temperature regimes are shown in Figure 9. The low-frequency intercepts on the Z' axis are interpreted as total resistance (sum of electrode, bulk, and grain-boundary contributions). The presence of the low-frequency intercepts on Z' suggests the nonblocking charge species of electrons and oxide ions.[57−59] The Arrhenius plot for the total conductivities of $Sr_2Ce_{1-x}Pr_xO_4$ in air is shown in Figure 10. Interestingly, the conductivity was found to increase with both temperature and Pr content. The increase of the conductivity with Pr content can be understood by the fact that Pr^{4+} ions have a lower reduction potential than that of Ce^{4+} ions; Pr^{4+} ions are more easily reduced comparing to Ce^{4+} ions under the same atmosphere as shown in the TGA analysis in Figure 11. The activation energies (0.6−0.7 eV) were found to increase slightly with increasing Pr content in $Sr_2Ce_{1-x}Pr_xO_4$ but are smaller than the typical activation energies of oxide ion

dx.doi.org/10.1021/ic301071x | Inorg. Chem. 2012, 51, 8973−8981

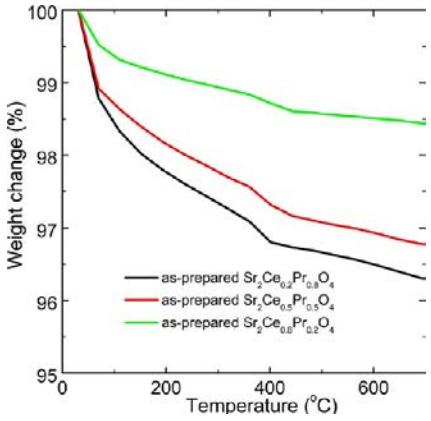

Figure 11. TGA analysis of the as-prepared $Sr_2Ce_{1-x}Pr_xO_4$ (x = 0.2, 0.5, 0.8) in air.

conduction (ca. 0.9 eV) and electron–hole (ca. 0.8 eV) in perovskite-type metal oxides.[60−62] The highest total conductivity was found to be 1.24×10^{-1} S cm^{-1} for $Sr_2Ce_{0.2}Pr_{0.8}O_4$ at 663 °C in air.

4. CONCLUSIONS

A new family of metal oxide with formula $Sr_2Ce_{1-x}Pr_xO_4$ ($0 \leq x \leq 1$) was developed as a mixed conductor for solid oxide fuel cells (SOFCs). The Sr_2PbO_4-type Sr_2CeO_4 undergoes thermal decomposition into perovskite-type $SrCeO_3$ and rock-salt-type SrO at 1400 °C. The thermally decomposed products can be converted back to Sr_2CeO_4 at 800 °C in air, confirmed by in-situ powder X-ray diffraction (PXRD). Such thermal decomposition was not observed in $Sr_2Ce_{1-x}Pr_xO_4$ at 1400 °C. All of the investigated samples were characterized by Rietveld refinement on PXRD, SAED, SEM, EDX, BVS, and EIS. Rietveld analysis reveals that both Ce and Pr ions are located on the *2a* site in *Pbam*. Conductivities increase with the amount of Pr ions in the lattices. The highest total (bulk, grain-boundary, and electrode) conductivity was found to be 1.24×10^{-1} S cm^{-1} for $Sr_2Ce_{0.2}Pr_{0.8}O_4$ at 663 °C in air.

■ ASSOCIATED CONTENT

Supporting Information

PXRD and EDX data for $Sr_2Ce_{1-x}Pr_xO_4$. This material is available free of charge via the Internet at http://pubs.acs.org.

■ AUTHOR INFORMATION

Corresponding Author

*E-mail: vthangad@ucalgary.ca.

Notes

The authors declare no competing financial interest.

■ ACKNOWLEDGMENTS

This research was supported through funding to the NSERC Solid Oxide Fuel Cell Canada Strategic Research Network from the Natural Science and Engineering Research Council (NSERC) and other sponsors listed at www.sofccanada.com. W.H.K. thanks Alberta Innovates–Technology Futures (AITF) for a graduate scholarship. We also thank the Canada Foundation for Innovation (CFI) for providing funding for the X-ray facility. We also thank Dr. Parvez for solving our single-crystalline samples and Dr. Tobias Fürstenhaupt for his help with electron diffraction studies.

■ REFERENCES

(1) Danielson, E.; Devenney, M.; Giaquinta, D. M.; Golden, J. H.; Haushalter, R. G.; McFarland, E. W.; Poojary, D. M.; Reaves, C. M.; Weinberg, W. H.; Di Wu, X. *J. Mol. Struct.* **1998**, *470*, 229–235.
(2) Danielson, E.; Devenney, M.; Giaquinta, D. M.; Golden, J. H.; Haushalter, R. C.; McFarland, E. W.; Poojary, D. M.; Reaves, C. M.; Weinberg, W. H.; Wu, X. D. *Science* **1998**, *279*, 837–839.
(3) Shi, L.; Zhang, H.; Li, C.; Su, Q. *RSC Adv.* **2011**, *1*, 298–304.
(4) Masui, T.; Chiga, T.; Imanaka, N.; Adachi, G. Y. *Mater. Res. Bull.* **2003**, *38*, 17–24.
(5) Ruddlesden, S. N. P., P. *Acta Crystallogr.* **1957**, *10*, 538–539.
(6) Ruddlesden, S. N. P., P. *Acta Crystallogr.* **1958**, *11*, 54–55.
(7) Gerlach, R. G.; Bhella, S. S.; Thangadurai, V. *Inorg. Chem.* **2009**, *48*, 257–266.
(8) Troemel, M. *Z. Anorg. Allg. Chem.* **1969**, *371*, 237–247.
(9) Troemel, M. *Naturwissenschaften* **1965**, *52*, 492–493.
(10) Murray, E. P. T., T.; Barnett, S. A. *Nature* **1999**, *400*, 649–651.
(11) Park, S.; Vohs, J. M.; Gorte, R. J. *Nature* **2000**, *404*, 265–267.
(12) Yang, L. W.; Shizhong; Blinn, K.; Liu, M.; Liu, Z.; Cheng, Z.; Liu, M. *Science* **2009**, *326*, 126–129.
(13) Trovarelli, A. *Catalysis by Ceria and Related Materials*; World Scientific Publishing Co.: River Edge, NJ, 2002.
(14) Singhal, S. C. K. *High Temperature Solid Oxide Fuel Cells Fundamentals, Design and Applications*; Elsevier: New York, 2003.
(15) Larminie, J.; Dicks, A. *Fuel Cell Systems Explained*, 2nd ed.; John Wiley: West Sussex, 2003.
(16) O'Hayre, R.; Cha, S.-W.; Colella, W.; Prinz, F. B. *Fuel Cell Fundamentals*; John Wiley: New York, 2006.
(17) Lide, D. R. *CRC Handbook of Chemistry and Physics*; CRC Press: Boca Raton, FL, 2003.
(18) Shirsat, A. N.; Kaimal, K. N. G.; Bharadwaj, S. R.; Das, D. *Thermochim. Acta* **2006**, *447*, 101–105.
(19) He, X.; Li, W.; Zhou, Q. *Mater. Sci. Eng. B: Solid State Mater. Adv. Technol.* **2006**, *134*, 59–62.
(20) Jiang, Y. D.; Zhang, F. L.; Summers, C. J.; Wang, Z. L. *Appl. Phys. Lett.* **1999**, *74*, 1677–1679.
(21) Serra, O. A.; Severino, V. P.; Calefi, P. S.; Cicillini, S. A. *J. Alloys Compd.* **2001**, *323*, 667–669.
(22) Viagin, O. M.; Andrey; Ganina, I.; Malyukin, Y. *Opt. Mater.* **2009**, *31*, 1808–1810.
(23) Masalov, A. A. V., O. G.; Ganina, I. I.; Malyukin, Yu. V. *Funct. Mater.* **2009**, *16*, 442–444.
(24) Perea-Lopez, N.; Gonzalez-Ortega, J. A.; Hirata, G. A. *Opt. Mater.* **2006**, *29*, 43–46.
(25) Tang, Y. G.; Hengping; Qin, Q. *Solid State Commun.* **2002**, *121*, 351–356.
(26) Perea, N. H., G. A. *Opt. Mater.* **2005**, *27*, 1212–1216.
(27) Yu, X. B.; He, X. H.; Yang, S. P.; Yang, X. F.; Xu, X. L. *Mater. Lett.* **2004**, *58*, 48–50.
(28) Lu, C.-H.; Chen, C.-T. *J. Sol–Gel Sci. Technol.* **2007**, *43*, 179–185.
(29) Ghildiyal, R.; Page, P.; Murthy, K. V. R. *J. Lumin.* **2007**, *124*, 217–220.
(30) Gomes, J.; Pires, A. M.; Serra, O. A. *Quim. Nova* **2004**, *27*, 706–708.
(31) Chavan, S. V.; Tyagi, A. K. *J. Mater. Res.* **2004**, *19*, 3181–3188.
(32) Shi, S. W.; Jiye; Li, J.; Zong, R.; Zhou, J. *Key Eng. Mater.* **2005**, *280–283*, 639–641.
(33) Xing, D. S.; Shi, J. X.; Gong, M. L. *Mater. Lett.* **2005**, *59*, 948–952.
(34) Hirai, T.; Kawamura, Y. *J. Phys. Chem. B* **2004**, *108*, 12763–12769.
(35) Hirai, T.; Kawamura, Y. *J. Phys. Chem. B* **2005**, *109*, 5569–5573.
(36) Tang, Y. X.; Guo, H. P.; Qin, Q. Z. *Solid State Commun.* **2002**, *121*, 351–356.
(37) Khollam, Y. B.; Deshpande, S. B.; Khanna, P. K.; Joy, P. A.; Potdar, H. S. *Mater. Lett.* **2004**, *58*, 2521–2524.
(38) Fiscus, J. E.; zur Loye, H. C. *J. Alloys Compd.* **2000**, *306*, 141–145.

(39) Hernandez-Velasco, J. *J. Magn. Magn. Mater.* **2007**, *310*, 1669–1671.
(40) Majumdar, S.; Lees, M. R.; Balakrishnan, G.; Paul, D. M. *J. Phys.: Condens. Matter* **2003**, *15*, 7585–7590.
(41) Toby, B. H. *J. Appl. Crystallogr.* **2001**, *34*, 210–213.
(42) Brown, I. D.; Altermat, D. *Acta Crystallogr.* **1985**, *B41*, 244–247.
(43) Hormillosa, C. H., S.; Stephen, T.; Brown, I. D.; 2.0 ed. 1993; www.ccp14.ac.uk/ccp/web-mirrors/i_d_brown/valence.exe.
(44) Brese, N. E.; O'Keefe, M. *Acta Crystallogr.* **1991**, *B47*, 192–197.
(45) Trzesowska, A.; Kruszynski, R.; Bartczak, T. J. *Acta Crystallogr.* **2004**, *B60*, 174–178.
(46) Palenik, G. J.; Hu, S.-Z. *Inorg. Chim. Acta* **2009**, *362*, 4740–4743.
(47) Roulhac, P. L.; Palenik, G. J. *Inorg. Chem.* **2003**, *42*, 118–121.
(48) Sheldrick, G. M. *Acta Crystallogr.* **2008**, *A64*, 112–122.
(49) Denton, A. R.; Ashcroft, N. W. *Phys. Rev. A* **1991**, *43*, 3161–3164.
(50) Ranlov, J.; Nielsen, K. *J. Mater. Chem.* **1994**, *4*, 867–868.
(51) Primak, W.; Kaufman, H.; Ward, R. *J. Am. Chem. Soc.* **1948**, *70*, 2043–2046.
(52) Harr, T. E. Univeristy of Syracuse (USA), 1947.
(53) Fang, S. B.; Lei; Wu, X.; Gao, H.; Chen, C.; Liu, W. *J. Power Sources* **2008**, *183*, 126–132.
(54) Bi, L. T.; Zetian; Liu, C.; Sun, W.; Wang, H.; Liu, W. *J. Membr. Sci.* **2009**, *336*, 1–6.
(55) Pasierb, P. W., M.; Komornicki, S.; Rekas, M. *J. Power Sources* **2009**, *194*, 31–37.
(56) Irvine, J. T. S. S., D. C.; West, A. R. *Adv. Mater.* **1990**, *2*, 132–138.
(57) Kan, W. H.; Trinh, T. T.; Fuerstenhaupt, T.; Thangadurai, V. *Can. J. Chem.-Rev. Can. Chim.* **2011**, *89*, 688–696.
(58) Kan, W. H.; Trinh, T. T.; Fuerstenhaupt, T.; Thangadurai, V. *ECS Trans.* **2011**, *35*, 1259–1266.
(59) Thangadurai, V.; Huggins, R. A.; Weppner, W. *J. Power Sources* **2002**, *108*, 64–69.
(60) Fabbri, E. D. E., A.; Di Bartolomeo, E.; Licoccia, S.; Traversa, E. *Solid State Ionics* **2008**, *179*, 558–564.
(61) Fabbri, E. P., D.; Traversa, E. *Chem. Soc. Rev.* **2010**, *39*, 4355–4369.
(62) Slade, R. C. T. S., N. *Solid State Ionics* **1991**, *46*, 111–115.